Intra-Vehicle UWB Channel Measurements and Statistical Analysis

Weihong Niu and Jia Li
ECE Department
Oakland University
Rochester, MI 48309, USA

Timothy Talty
GM R & D Planning
General Motors Corporation
Warren, MI 48092, USA

***Abstract*—Ultra-wideband (UWB) technique attracts attention from automotive manufacturers as a potential way to construct intra-vehicle wireless sensor network. This paper reports our preliminary effort in measuring and modeling the UWB propagation in the commercial vehicle environment. Two cases of time domain channel measurement results are reported. In one case, the antennas are inside the engine compartment. In the other case, both antennas are beneath the chassis. It is observed that clustering phenomenon exists in the former case but not in the latter one. Different channel models are used to describe UWB propagation in the two cases and model parameters are found by statistically analyzing the impulse responses.**

Keywords-UWB; intra-vehicle; channel model; statistical analysis; impulse response

I. INTRODUCTION

Modern vehicles are being deployed with an ever increasing number of sensors for the purpose of safety, comfort or convenience. Cables used to connect these sensors in a commercial car can amount to 1000 meters and the wire harness can add 50kg to its weight [1]. This fact negatively affects the cost, fuel economy and environment friendliness required for vehicles nowadays. At the same time, it also brings complication to vehicle design. Thus, wireless network is proposed as a possible way to replace the current cable system for the transmission of sensor control and data information [2]. The intra-vehicle environment for transmitting wireless signals features short range and big challenge in implementing a wireless sensor network within vehicles is to provide comparable reliability, data rate and transmission delay as the existing wire network does.

Ultra-Wideband (UWB) signal is defined as the wireless radio which takes a bandwidth larger than 500MHz or a fractional bandwidth greater than 25%. In USA, FCC authorized the use of UWB signals in the frequency range 3.1GHz to 10.6GHz with a power spectral density emission limited within -41.3dBm/MHz [3]. Due to its extremely wide transmission bandwidth, UWB technique provides fine delay resolution in time domain, which means the lack of significant multipath fading. In addition, UWB signals also demonstrate strong resistance to narrow band interference. These features make UWB a promising technique in constructing the intra-vehicle wireless sensor network and attract great attention from commercial automotive manufacturers.

This work is supported by the NSF under Grant No. 0721813.

In order to design a UWB communication system, it is essential to understand the UWB signal propagation characteristics in the desired environment. A lot of measurement experiments have been performed for indoor and outdoor environments in the UWB literature, but very few measurements have been reported for intra-vehicle environment. This paper presents our preliminary work in measuring and characterizing UWB multipath propagation for a commercial car environment. The data collected from the experiment is statistically analyzed and the differences of our measurements from S-V model are identified.

II. UWB INTRA-VEHICLE PROPOGATION EXPERIMENTS

The measurement is performed in time domain by sounding the channel with narrow pulses. Fig. 1 illustrates the block diagram of the measurement apparatus. At the transmitting side, a Wavetek sweeper and an impulse generator from Picosecond work together to create narrow pulses of width 100 picoseconds as input to a scissors-like transmitting antenna. At the receiving side, a 10G Hz bandwidth oscilloscope from Tektronix is used to record the signals output from the receiving antenna. In Fig. 1, three cables of same length are used. One is to connect the receiving antenna to the oscilloscope, another one connects the impulse generator output to the transmitting antenna, and the third one connects the impulse generator output to the trigger input of the oscilloscope for the purpose of time synchronization. In this way, all recorded waveforms have the same time reference point so that their propagation delay can be measured.

The vehicle used in our experiment is a 2002 Ford Taurus parking in a large empty garage built from concrete and steel. In accordance with the sensor locations in the existing wire sensor network, two cases of measurements are made. In the first case, the antennas are located beneath the chassis and 15cm above ground, facing each other. This is line-of-sight case (LOS). As illustrated in Fig. 2, the transmitting antenna stays at the same location while the receiving antenna is moved

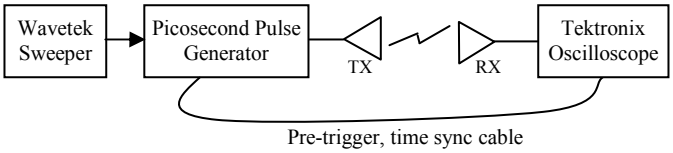

Figure 1. Diagram of channel sounding apparatus.

978-1-4244-2324-8/08/$25.00 © 2008 IEEE.

to 10 spots, with 5 equidistant (70cm) ones along each side of the car. Six waveforms are recorded by the oscilloscope for each spot when the pulse is repeatedly transmitted. In the second case, both antennas are put inside the engine compartment with the hood closed. This is the non-LOS case, with iron auto parts sitting between the transmitting and receiving antennas. Similarly, six waveforms are recorded for each of the 5 locations of the receiving antenna as illustrated in Fig. 3.

III. DECONVOLUTION AND MULTIPATH CHANNEL MODELS

To get the channel impulse responses (CIRs) from the measured data, the subtractive deconvolution technique, or CLEAN algorithm, is used [4]. This algorithm assumes that any received multipath signal r(t) is the sum of a shape p(t). In our case, p(t) is the received signal when the two antennas are 1m apart from each other. It is shown in Fig. 4. The impulse response is deconvolved by iteratively subtracting p(t) from r(t). In each iteration, the peak in the normalized cross correlation of p(t) and r(t) is found. Then p(t) is multiplied by the peak value and an iteration factor, and the result is subtracted from r(t). The iteration stops until the energy of r(t) falls below a threshold. Examples of the resulted impulse responses are shown in Fig. 5 and Fig. 6 for the measured data in LOS and non-LOS cases, when the iteration factor is set to 0.01 and the threshold in the stop criteria is 0.05.

Observation of the waveforms and impulse responses reveals that there is no clustering phenomenon for the measurements made beneath the chassis. But paths arrive in clusters for the experiments performed inside engine compartment. Accordingly, non-clustering multipath model of

$$h(t) = \sum_{k=0}^{\infty} \alpha_k \exp(j\theta_k)\delta(t-\tau_k) \qquad (1)$$

is used to describe the impulse response for the former case [5]. α_k, θ_k and τ_k are the positive path gain, the phase shift and the path arrival time delay for each multipath component (MPC). And the clustering S-V model as below is chosen for the latter [6]:

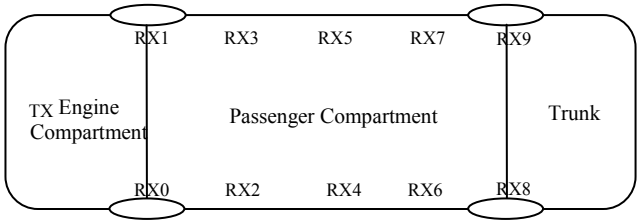

Figure 2. Antenna locations beneath chassis.

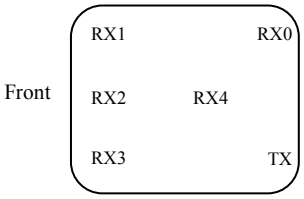

Figure 3. Antenna locations inside engine compartment.

$$h(t) = \sum_{l=0}^{\infty}\sum_{k=0}^{\infty} \alpha_{kl} \exp(j\theta_{kl})\delta(t-T_k-\tau_{kl}) \qquad (2)$$

where α_{kl}, θ_{kl} and τ_{kl} are the positive gain, the phase shift and the relative time delay of the *kth* path within the *lth* cluster and T_k is the time delay of the *lth* cluster relative to the first path in the first cluster. The parameters T_k and τ_{kl} observe the Poisson law [6]:

$$p(T_l \mid T_{l-1}) = \Lambda \exp[-\Lambda(T_l - T_{l-1})], \quad l > 0 \qquad (3)$$

$$p(\tau_{kl} \mid \tau_{(k-1)l}) = \lambda \exp[-\lambda(\tau_{kl} - \tau_{(k-1)l})], \quad k > 0 \qquad (4)$$

where Λ and λ are the arrival rate of clusters and paths within clusters, respectively. In addition, the mean square values of the path gains are described by:

$$\overline{\alpha_{kl}^2} = \overline{\alpha_{00}^2} \exp(-T_l/\Gamma)\exp(-\tau_{kl}/\gamma) \qquad (5)$$

in which $\overline{\alpha_{00}^2}$ is the average power gain of the first path in the first cluster. Γ and γ are the power decay constants of clusters and the paths within clusters, indicating the corresponding decaying speed. Normally γ is smaller than Γ [6].

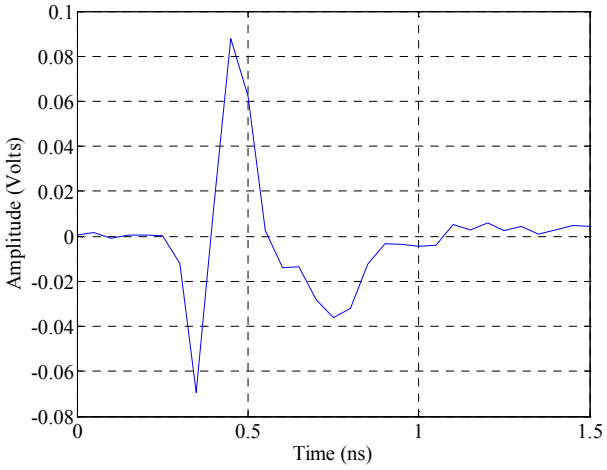

Figure 4. Observed signal shape at 1m away from transmitting antenna.

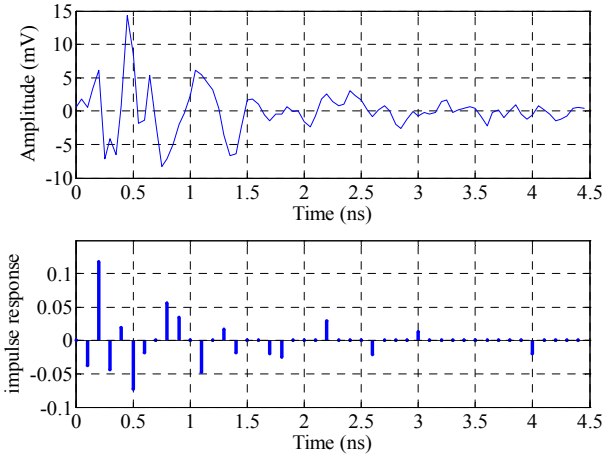

Figure 5. One observed waveform and deconvolved CIR for LOS case.

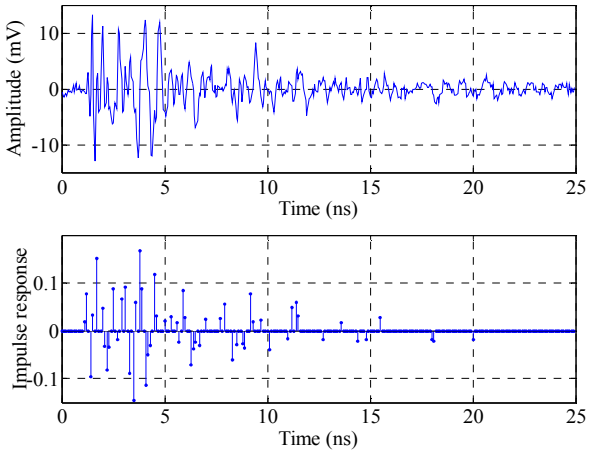

Figure 6. One observed waveform and deconvolved CIR for non-LOS case.

IV. STATISTICAL ANALYSIS ON MEASURED DATA

In this section, the channel impulse responses are statistically analyzed to provide small-scale characterization of the intra-vehicle UWB channel. For those measured data showing clustering phenomenon, clusters are identified manually so that MPCs with similar time-of-arrivals are divided into the same cluster.

A. RMS Delay Spread Distribution

As a good measure of the multipath spread, root-mean-square (RMS) delay spread is calculated for all impulse responses. The cumulative distribution functions (CDFs) of RMS delay spread for the measurements beneath chassis and inside engine compartment are plotted in Fig. 7. Accordingly, the mean RMS delay spread for the two measurement cases is 0.3441 ns and 3.1112 ns respectively.

B. Inter-path and Inter-cluster Arrival Times

The inter-path and inter-cluster arrival times are modeled as Poisson arrival processes with fix rates λ and Λ respectively [6].

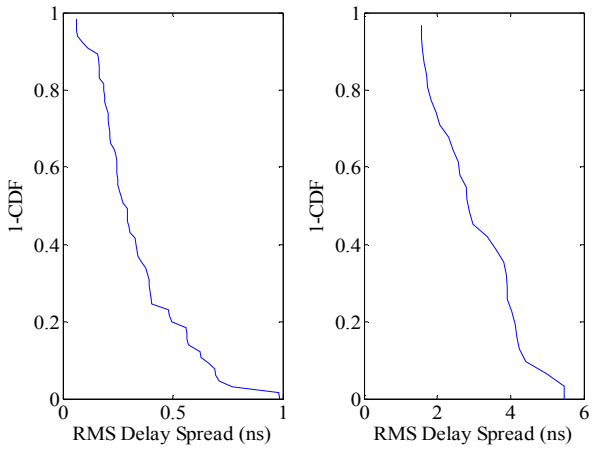

Figure 7. Cumulative distribution of the RMS delay spread for chassis (left) and engine compartment (right) measurements.

They are estimated by finding the cumulative distribution functions of the path and cluster arrival intervals. $1/\lambda$ and $1/\Lambda$ equal the mean values of the exponential distribution functions best fitting these CDFs. In our experiments, $1/\lambda$ calculated from the measured data beneath chassis is 0.2245 ns. For the engine compartment measurements, $1/\lambda$ is 0.3341 and $1/\Lambda$ equals 2.6281 ns. The semilog plots of these CDFs with their best fits are shown in Fig. 8, Fig. 9 and Fig. 10.

C. Distributions of Path and Cluster Amplitudes

Before the empirical CDF of the path or cluster amplitude is calculated, each CIR is normalized by setting the amplitude of the peak path to be one. The amplitudes of the other paths in this CIR are expressed in values relative to it. In addition, the peak amplitude within a cluster is identified as the amplitude of the cluster. To model the path and cluster amplitude distributions, the CDFs are matched to Rayleigh and lognormal distributions via maximum likelihood estimation. For the measurements from beneath chassis and inside engine compartment, parameters of the best fit Rayleigh

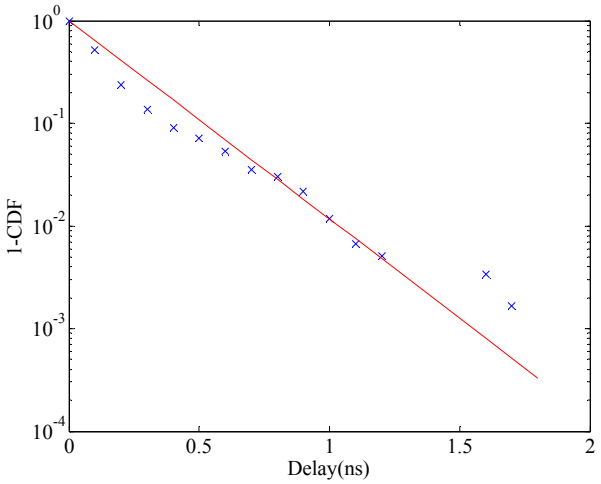

Figure 8. CDF of inter-path arrival times and the best fit exponential distribution ($1/\lambda$=0.2245ns) for measurements beneath chassis.

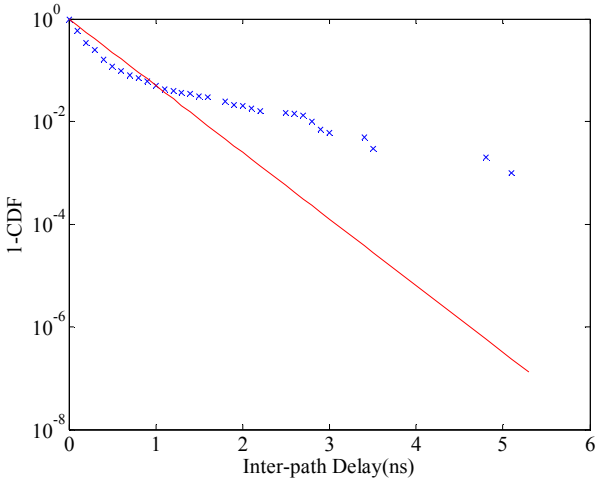

Figure 9. CDF of inter-path arrival times and the best fit exponential distribution ($1/\lambda$=0.3341ns) for measurements inside engine compartment.

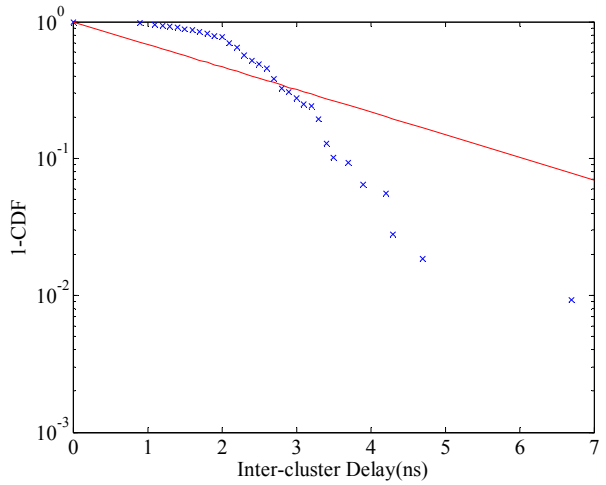

Figure 10. CDF of inter-cluster arrival times and the best fit exponential distribution (1/Λ=2.6281ns) for measurements inside engine compartment.

and lognormal distributions are listed in Table 1. The fitting results reveal that lognormal is a better fit than Rayleigh in all cases. Fig. 11, Fig. 12 and Fig. 13 are the plots of the CDFs with Rayleigh and lognormal distributions overlaid.

D. Path and Cluster Power Decay

For the measured data from beneath the chassis, when the deconvolved CIRs are normalized in a way so that their first paths have amplitudes of one and time delay of zero, the average relative path powers corresponding to their relative time delays are superimposed in Fig. 14. The power decay constant γ, defined in S-V model, is found by finding a linear curve best fitting the data in the least squares sense. γ equals the absolute reciprocal of the curve's slope and for measurements beneath chassis, its value is 0.5543 ns.

For the measured data from engine compartment, normalization is performed on all clusters so that the first path in each cluster has amplitude of one and a time delay of zero. The superimposition of relative path powers corresponding to their relative delays from all clusters is plotted in Fig. 15. The best fit curve in the least squares sense gives the intra-cluster path power decay constant γ a value of 4.9931 ns. Similarly, in order to get the cluster power decay constant Γ, each IR is normalized in a way that its first cluster has amplitude one [7]. Here cluster amplitude is defined as the peak amplitude within a cluster. Fig. 16 shows the normalized cluster powers and their time delay. The cluster decay constant Γ is 9.9628 ns.

TABLE I. STANDARD DEVIATION OF RAYLEIGH AND LOGNORMAL FIT TO PATH AND CLUSTER DISTRIBUTION

CDF	Standard Deviation	
	Rayleigh	***Lognormal***
Path amplitude (beneath chassis)	0.3566	6.2675
Path amplitude (engine compartment)	0.2405	5.1768
Cluster amplitude (engine compartment)	0.4773	4.8424

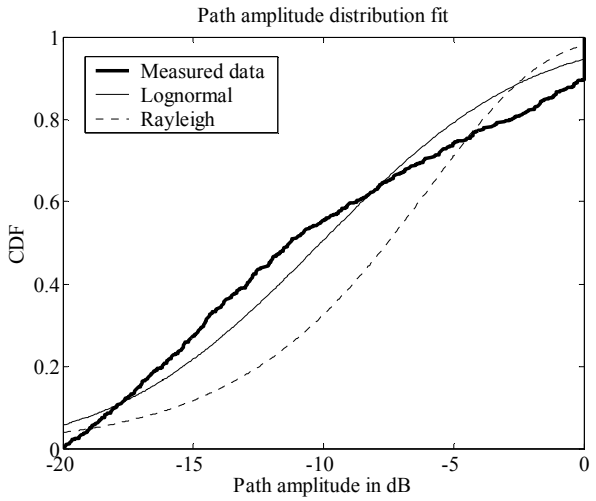

Figure 11. Path amplitude CDF with the best fit Rayleigh and lognormal distributions for measurements beneath chassis.

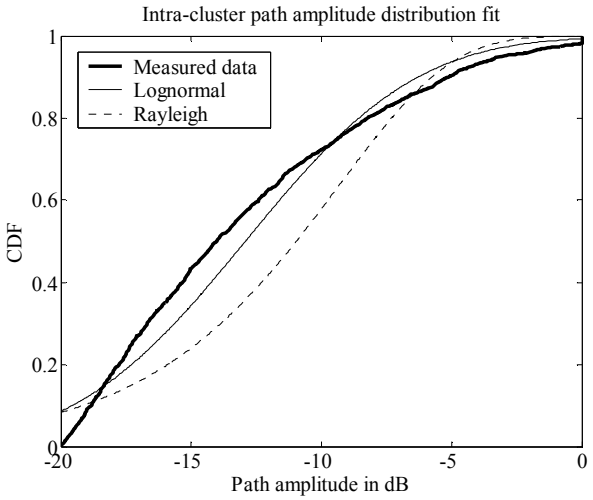

Figure 12. Intra-cluster path amplitude CDF with the best fit Rayleigh and lognormal distributions for measurements inside engine compartment.

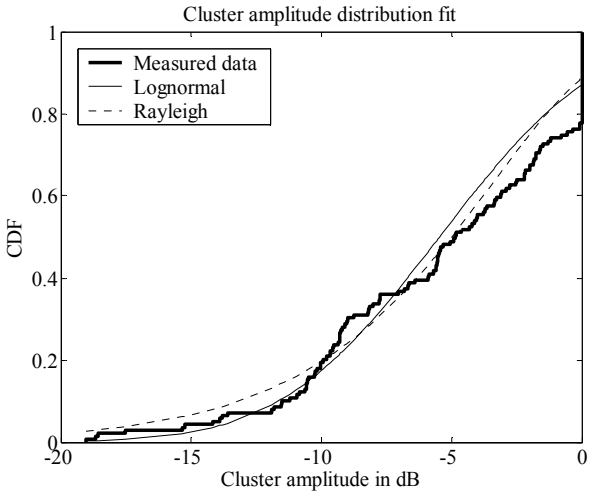

Figure 13. Cluster amplitude CDF with the best fit Rayleigh and lognormal distributions for measurements inside engine compartment.

V. CONCLUSION

The statistical analysis of our measured data shows that in the intra-vehicle environment, the path or cluster arrival rates are greatly larger than those reported for indoor environment while the path or cluster power decay constants are much smaller [8] [9] [10]. This is due to the short range of intra-vehicle propagation. In addition, the RMS delay spreads of our measurements are also a lot less than those of the indoor UWB propagation [11] [12], which indicate smaller intersymbol interference.

It is observed from Fig. 14, Fig. 15 and Fig. 16 that in our measurement environment, unlike what is defined in S-V model, the first path or first cluster does not always have the largest power. Therefore, S-V model, specifically (5), needs modification to characterize the observation. This will be included in our future work. Moreover, channel simulation will be implemented later to evaluate the effectiveness of the channel models in characterizing the intra-vehicle UWB propagation.

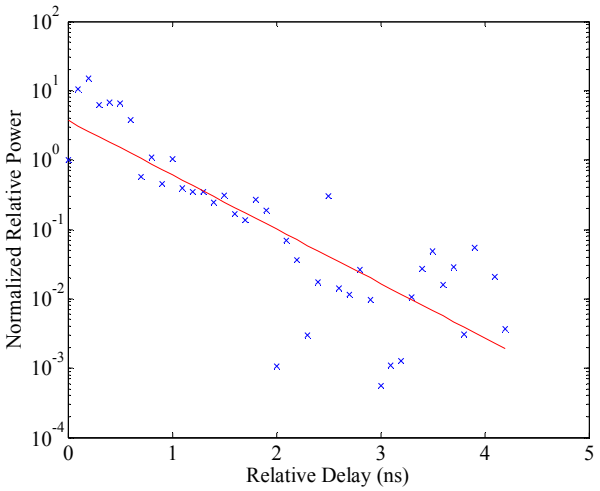

Figure 14. Average normalized path power decay corresponding to time delay for measured data from beneath chassis (γ = 0.5543 ns)

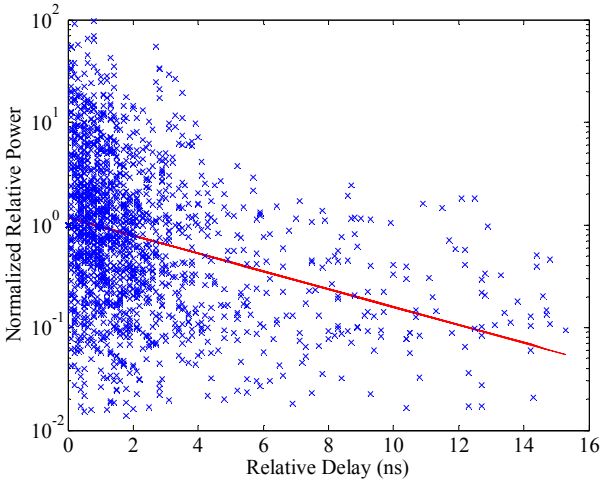

Figure 15. Normalized intra-cluster path power decay corresponding to time delay for measurements from engine compartment (γ = 4.9931 ns).

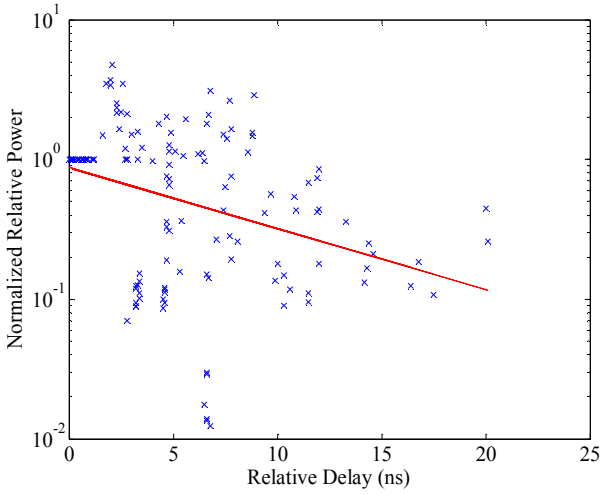

Figure 16. Normalized cluster power decay corresponding to time delay for measurements from engine compartment (Γ = 9.9628 ns).

REFERENCES

[1] G. Leen and D. Hefferna, "Vehicles without wires," *Automotive Electronics, Computing and Control Engineering Journal*, pp. 205-211, Oct. 2001.

[2] T. ElBatt, C. Saraydar, M. Ames, and T. Talty, "Potential for intra-vehicle wireless automotive sensor networks," *2006 IEEE Sarnoff Symposium*, 27-28 March 2006, Princeton, NJ.

[3] First report and order 02-48, Federal Communications Commission, 2002.

[4] R. G. Vaughan and N. L. Scott, "Super-resolution of pulsed multipath channels for delay spread characterization," *IEEE Transactions on Communications*, vol. 47, pp. 343-347, March 1999.

[5] J. G. Proakis, *Digital Communications 5TH Edition*. New York: McGraw-Hill, 2007.

[6] A. Saleh and R. A. Valenzuela, "A statistical model for indoor multipath propagation," *IEEE Journal on Selected Areas in Communications*, vol. 5, pp. 128-137, Feb. 1987.

[7] C.-C Chong and S. K. Yong, "A generic statistical-based UWB channel model for high-rise apartments," *IEEE Transactions on Antennas and Propagation,* vol. 53, pp. 2389-2399, Aug. 2005.

[8] R. J.-M. Cramer, R. A. Scholtz, and M. Z. Win, "Evaluation of an ultra-wide-band propagation channel," *IEEE Transactions on Antennas and Propagation*, vol. 50, pp. 561-570, May 2002.

[9] Q. Spencer, M. Rice, B. Jeffs, and M. Jensen, "A statistical model for angle of arrival in indoor multipath propagation," *IEEE 47th Vehicular Technology Conference*, vol. 3, pp. 1415–1419, May 1997.

[10] S. S. Ghassemzadeh, R. Jana, C. W. Rice, W. Turin, and V. Tarokh, "Measurement and modeling of an ultra-wide bandwidth indoor channel," *IEEE Transactions on Communications*, vol. 52, pp. 1786–1796, 2004.

[11] J. Foerster, "Channel modeling sub-committee report final," IEEE P802.15-02/490r1-SG3a, Feb. 2003.

[12] A. F. Molisch, K. Balakrishnan, D. Cassioli, C.-C Chong, S. Emami, A. Fort, J. Karedal, J. Kunisch, H. Schantz, U. Schuster, and K. Siwiak, "IEEE 802.15.4a channel model - final report," IEEE 802.15-04-0662-00-004a, Nov. 2004.